Journal of Alloys and Compounds 495 (2010) 260–264

Contents lists available at ScienceDirect

Journal of Alloys and Compounds

journal homepage: www.elsevier.com/locate/jallcom

Structural evolution of Fe–50 at.% Al powders during mechanical alloying and subsequent annealing processes

Sh. Ehtemam Haghighi [a], K. Janghorban [a], S. Izadi [b,*]

[a] Department of Materials Science and Engineering, School of Engineering, Shiraz University, Zand Blvd, 7134851154 Shiraz, Iran
[b] Department of Material Science and Engineering, Shahid Bahonar University of Kerman, 76135-133 Kerman, Iran

ARTICLE INFO

Article history:
Received 5 November 2009
Received in revised form 27 January 2010
Accepted 29 January 2010
Available online 6 February 2010

Keywords:
Nanostructured materials
Mechanical alloying
X-ray diffraction
Order–disorder effects

ABSTRACT

Iron aluminides, despite having desirable properties like excellent corrosion resistance, present low room-temperature ductility and low strength at high temperatures. Mechanical alloying as a capable process to synthesize nanocrystalline materials is under consideration to modify these drawbacks. In this study, the microstructure of iron aluminide powders synthesized by mechanical alloying and subsequent annealing was investigated. Elemental Fe and Al powders with the same atomic percent were milled in a planetary ball mill for 15 min to 100 h. The powder milled for 80 h was annealed at temperatures of 300, 500 and 700 °C for 1 h. The alloyed powders were disordered Fe(Al) solid solutions which were transformed to FeAl intermetallic after annealing. The effect of the milling time and annealing treatment on structural parameters, such as crystallite size, lattice parameter and lattice strain was evaluated by X-ray diffraction. Typically, these values were 15 nm, 2.92 Å and 3.1% for the disordered Fe(Al) solid solution milled for 80 h and were 38.5 nm, 2.896 Å and 1.2% for the FeAl intermetallic annealed at 700 °C, respectively.

1. Introduction

FeAl intermetallic compounds present desirable properties, such as high specific strength, high specific stiffness and good strength at intermediate temperatures. They have relatively high electrical resistivity, low thermal conductivity, and excellent corrosion resistance at elevated temperatures under oxidizing, carburizing and sulfidizing atmospheres [1–3]. These features make the FeAl a very attractive material for structural and coating applications at elevated temperatures in hostile environments [4]. Additionally, its tensile strength is comparable to that of austenitic and ferritic steels [5,6]. The FeAl intermetallic compound is lighter than steels or Ni-based alloys; therefore, it could be considered as a substitute for stainless steels or Ni-based superalloys [1]. However, it has not been developed commercially due to low ductility at room temperature and low mechanical strength above 600 °C [7,8]. It has been found that restricted cross-slip and intense planar slip are the key features of low ductility in B2-structured compounds such as FeAl [11]. Intense planar slip can lead to crack nucleation from dislocation pile-ups at low overall strains. The general approach to this problem is to prevent intense planar slip by homogenizing slip through dispersing slip to other slip planes or, possibly, other slip systems, and to limit the length of dislocation pile-ups [11]. This can be performed by reducing the crystallite size to the nanometer range or by introducing fine hard incoherent particles to induce slip homogenization [9–12].

Mechanical alloying (MA) is a viable technique of producing nanostructured materials on an industrial scale [13]. MA is a solid-state dry milling process that through a micro-sandwich morphology leads to the mixing of elemental powders and eventual alloy formation [14]. This technique allows one to overcome problems, such as large differences in melting points of the alloying components and unwanted segregation or evaporation that could occur during melting and casting [1,2]. In recent years, a number of studies have been reported on mechanical alloying of FeAl. For instance, Krasnowski et al. [2] investigated the effect of milling time on the crystallite size, lattice strain and lattice parameter of Fe–50 at% Al powder mixture. According to their results, with increasing milling time, the lattice parameter increased but the crystallite size and lattice strain increased up to 6 h and then decreased and finally after 10 h remained constant. In addition, Wolski et al. [15] studied the effect of milling conditions on the FeAl intermetallic formation by MA. According to their investigation, the crystallite size decreased and the lattice stresses increased with increasing speed and time of milling. Guo and Shi [16] investigated the structural evolution of nanocrystalline FeAl compound during MA. As their results showed, the crystallite size decreased and the lattice strain increased with milling time. They also studied the effect of annealing on XRD patterns of the mechanically

* Corresponding author. Tel.: +98 917 138 3812; fax: +98 711 230 7293.
E-mail address: saideh_izadi177@yahoo.com (S. Izadi).

0925-8388/$ – see front matter © 2010 Elsevier B.V. All rights reserved.
doi:10.1016/j.jallcom.2010.01.145

alloyed powders. During annealing, the superlattice reflections of the ordered structure appeared and the broadening of reflection peaks decreased.

In this work, microstructural changes of Fe–50 at.% Al powder mixture taking place during MA and subsequent annealing were studied in detail by X-ray diffraction (XRD), scanning electron microscopy (SEM) and transmission electron microscopy (TEM). Generally, overlapping XRD reflections, leading to asymmetric peaks, make the analysis difficult. In this work deconvolution of the asymmetric peaks was performed by Fityk software. The morphological and microstructural evolutions were determined and interpreted according to processing and metallurgical parameters.

2. Experimental procedure

Elemental Fe (>99%) and Al (>99.9%) powders (Fe was supplied by MERC and Al by BDH) with a nominal composition of Fe–50 at.% Al were milled in a planetary ball mill under argon. The milling operation was performed at 300 rpm for times ranging from 15 min to 100 h. In all the experiments, seven hardened steel balls with a diameter of 20 mm were used with 4.67 g powder mixture, i.e. the ball-to-powder weight ratio was 50:1. To observe the microstructural changes during MA, the powders milled for 15 min, 1 h and 80 h were compacted by a load of 30 kN to disks of 10 mm in diameter and 2 mm thickness. They were polished and then etched in Nital 2% solution to remove any surface contamination. The microstructural morphology of the compacted samples was characterized by SEM (Leica Cambridge model).

The 80 h milled powder was annealed in a sealed quartz tubes evacuated to 10^{-3} torr for 1 h at 300, 500 and 700 °C. Annealing was performed in a Carbulite Furnace with a heating rate of 15 °C/min. After annealing, the samples were air-cooled to room temperature. Phase changes that occurred in the powders during milling and annealing were investigated by X-ray diffraction using Philips Analytical PC-APD with a CuKα radiation (λ = 0.1542 nm). The step size and step time were 0.05° and 1 s/step, respectively. The lattice parameter, long-range order parameter, crystallite size and lattice strain were calculated from the XRD data.

The asymmetric peaks in the XRD patterns were fitted with pairs of overlapping symmetric peaks of Fe and Fe(Al) solid solution. It was performed by pseudo-Voight function with the help of Fityk [17] computer software. This fitting method permits the deconvolution of asymmetric diffraction profiles and the analysis of the peaks related to each phase. From the XRD patterns, the crystallite size, D, and the lattice strain, ε, of the samples were calculated using the Williamson–Hall equation:

$$B\cos\theta = \frac{k\lambda}{D} + 2\varepsilon\sin\theta \quad (1)$$

where B is the full width at half maximum (FWHM) of a diffraction peak, k is a constant, λ is the X-ray wavelength, and θ is the Bragg angle. According to Eq. (1), $B\cos\theta$ vs. $\sin\theta$ were plotted. Then, the crystallite size and lattice strain were calculated from the intercept and slope of this line, respectively [18]. The lattice parameter, a, of each phase was estimated according to the peak position of phases and by the use of the following equation [19]:

$$a = \frac{\lambda\sqrt{h^2+k^2+l^2}}{2\sin\theta} \quad (2)$$

The long-range order parameter, S, was determined by a comparison of the relative intensities of superlattice ($h+k+l$ odd) and fundamental ($h+k+l$ even) peaks of the annealed powders with respect to the well-annealed reference material according to:

$$S^2 = \frac{I_{S(\mathrm{dis})}/I_{F(\mathrm{dis})}}{I_{S(\mathrm{ord})}/I_{F(\mathrm{ord})}} \quad (3)$$

where $(I_S/I_F)_{\mathrm{dis}}$ and $(I_S/I_F)_{\mathrm{ord}}$ are the ratios of the integrated intensities (peak area) of the superlattice reflection to the fundamental line for the disordered (dis) and reference (ord) powders, respectively [20,21]. For the determination of S (2 0 0) and (1 0 0) reflections were chosen to minimize any texture effect [21]. To verify the validity of the XRD method in determining the crystallite sizes, transmission electron microscopy (TEM, JEOL-JEM 2010) was used. The TEM sample preparation was performed by dispersing the powder particles in ethanol and dropping down them in a copper rigid.

3. Results

Fig. 1 shows variations of the XRD pattern of the initial powder mixture with the milling time. According to these results, with increasing the milling time to 50 h, the intensity of Al peaks decreases gradually; however, Fe diffraction peaks slightly shift to lower angles and become asymmetric and broadened. It is due to the appearance of new broad peaks on the left side of the Fe

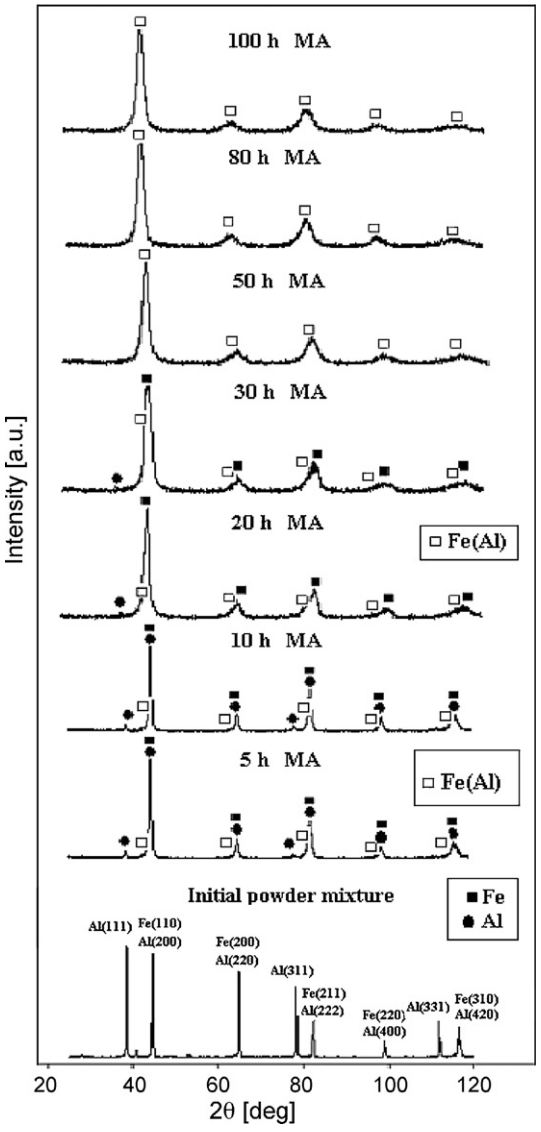

Fig. 1. XRD patterns of the initial powder mixture and the powders milled for the different times.

peaks. These additional peaks are attributed to a new phase, Fe(Al) solid solution which possesses the same structure as Fe, but is characterized by a slightly larger unit cell parameter [2]. The asymmetric peaks can be fitted by two overlapping symmetric peaks; the more intense peak is related to Fe and the lesser one is Fe(Al) [2]. This deconvolution was carried out by the pseudo-Voight function which provides the best data fit, as represented in Fig. 2(a) for the (2 1 1) peak. More focus on the XRD profiles of Fig. 1 reflects that after 50 h of MA, the strongest Al peak, (1 1 1), disappears completely and the peaks get symmetric (Fig. 2(b)). This indicates that all the Fe and Al peaks were replaced by those of the Fe(Al) solid solution. But under no circumstances, the superlattice reflections of the FeAl ordered structure (B2) were detected. This suggests that MA does not result in ordering under the experimental conditions of this work.

The lattice parameter of the Fe and Fe(Al) phases as a function of milling time is depicted in Fig. 3. For 5, 10, 20 and 30 h, the Fe and Fe(Al) lattice parameters were calculated according to their diffraction (2 1 1) peak position. However, for 50, 80 and 100 h of milling because of the existence of one phase, only the Fe(Al) lattice parameter was estimated. It can be seen that the lattice parameter of both phases increases with increasing the milling time; and the lattice

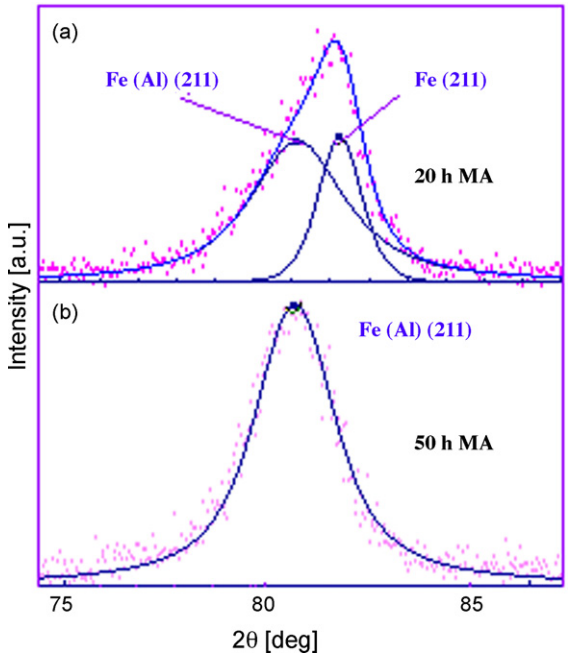

Fig. 2. (a) Deconvolution of Fe and Fe(Al) peaks after 20 h milling and (b) symmetric profile after 50 h MA process.

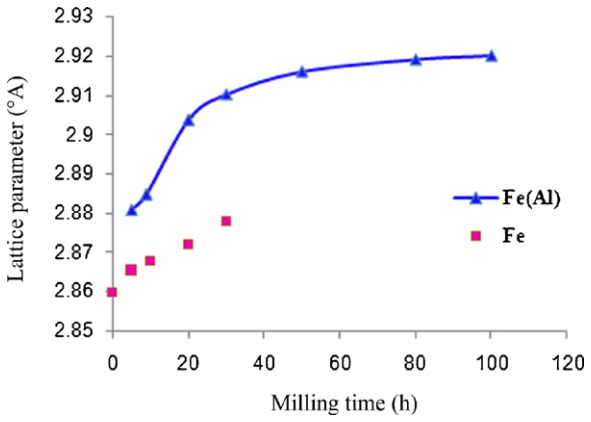

Fig. 3. Lattice parameter of the Fe and Fe(Al) phases as a function of milling time.

parameter of the Fe(Al) solid solution increases to 50 h milling and then reaches a steady value of 2.92 Å.

To establish the Williamson–Hall plot, XRD peaks which are elastically isotropic are required to be selected. The elastic modulus of iron single crystal in ⟨1 1 0⟩ and ⟨2 1 1⟩ directions is equal to 219 GPa and in ⟨1 0 0⟩ and ⟨3 1 0⟩ directions is 130 GPa. According to the Hook's law, it is expected that the strain in ⟨1 0 0⟩ and ⟨3 1 0⟩ directions to be larger than in ⟨1 1 0⟩ and ⟨2 1 1⟩ directions; therefore, the broadening of diffraction planes (2 0 0) and (3 1 0) is larger than (1 1 0), (2 1 1) and (2 2 0) planes [22]. If all the five peaks are employed for the Williamson–Hall plot, the *R*-squared would be lower than the case in which only (1 1 0), (2 1 1) and (2 2 0) planes are used. Thus, for the Williamson–Hall plots, only (1 1 0), (2 1 1) and (2 2 0) diffraction peaks were used. For instance, the Williamson–Hall plots of the sample milled for 50 h by the five and three peaks are shown in Fig. 4.

The crystallite size and lattice strain are plotted as a function of milling time in Fig. 5, obtained from the Williamson–Hall analyses. They suggest that the crystallite size and lattice strain of Fe(Al) increase from 11.3 nm and 2.4% (for 20 h) to 23 nm and 3.3% (for 50 h), respectively, then decrease to 15 nm and 2.9% (for 80 h), and

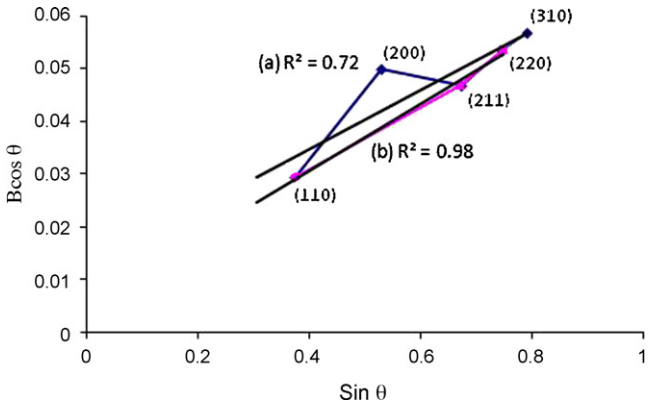

Fig. 4. Williamson–Hall plots of the powder milled for 50 h; using the data of the five peaks (a) and the three peaks (b).

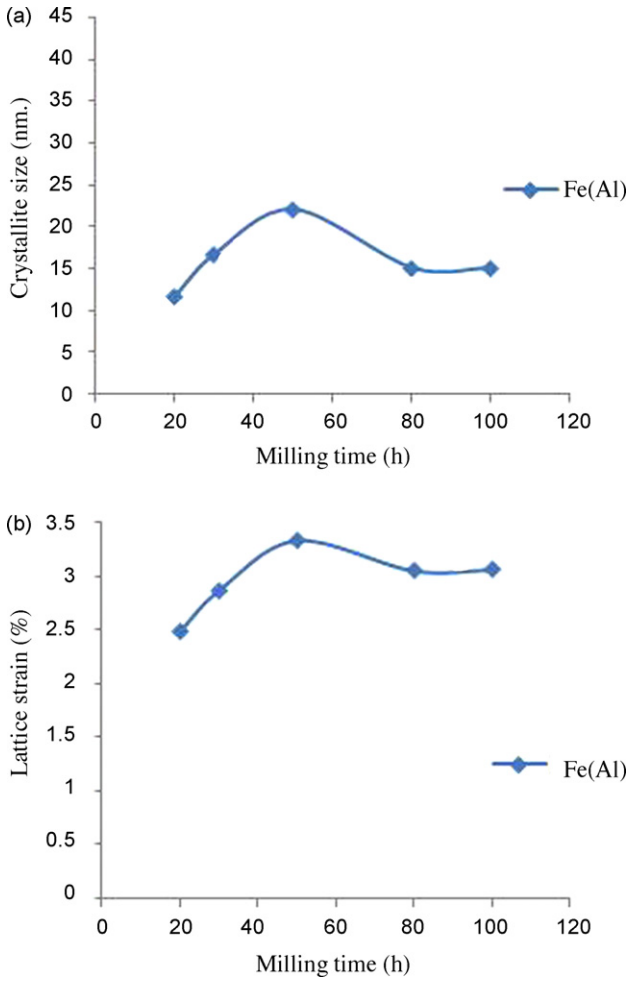

Fig. 5. Estimated crystallite size (a) and lattice strain (b) as a function of milling time.

remain nearly constant to 100 h. The TEM micrograph and corresponding selected area diffraction (SAD) pattern of the powder milled for 80 h are presented in Fig. 6, confirming the validity of the XRD analysis in the crystallite size determination.

Fig. 7 demonstrates the SEM morphology of the powders milled for 15 min, 1 h and 80 h after compaction and polishing (backscatter electron mode). Since the backscatter electron signal in SEM is sensitive to atomic number, the contrast in the grayness of zones is an indication of their different chemical compositions. The micro-

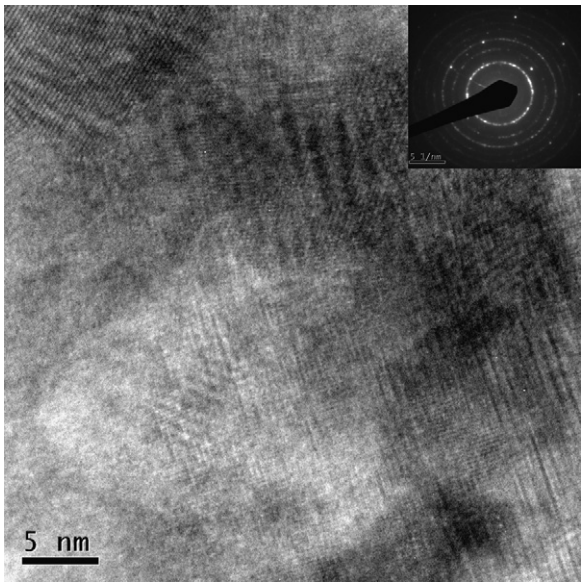

Fig. 6. TEM micrograph and corresponding SAD pattern of the powder milled for 80 h.

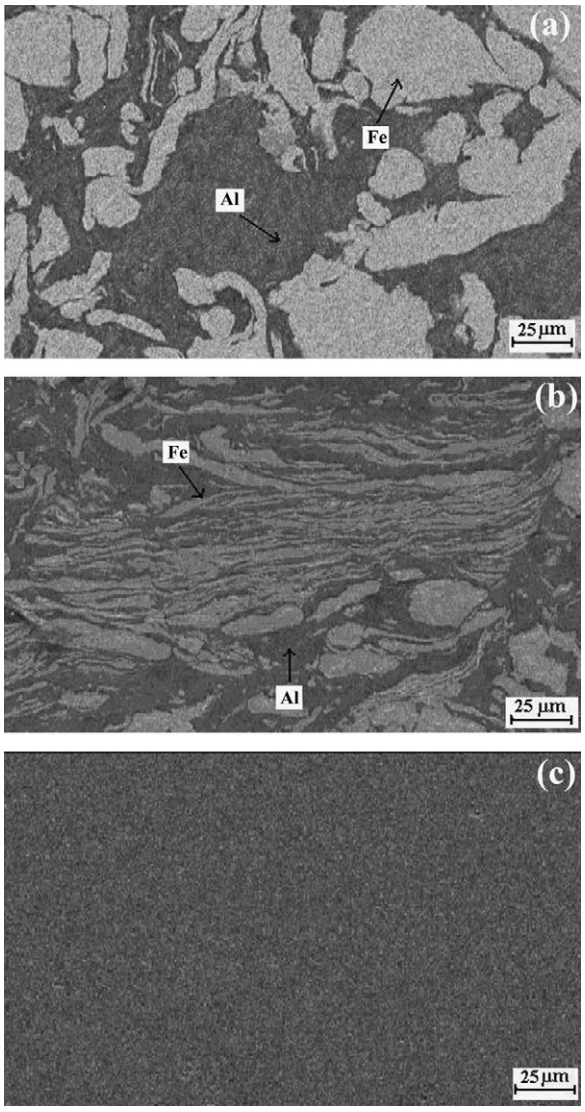

Fig. 7. SEM micrograph of the compacted and polished samples milled for 15 min (a), 1 h (b) and 80 h (c).

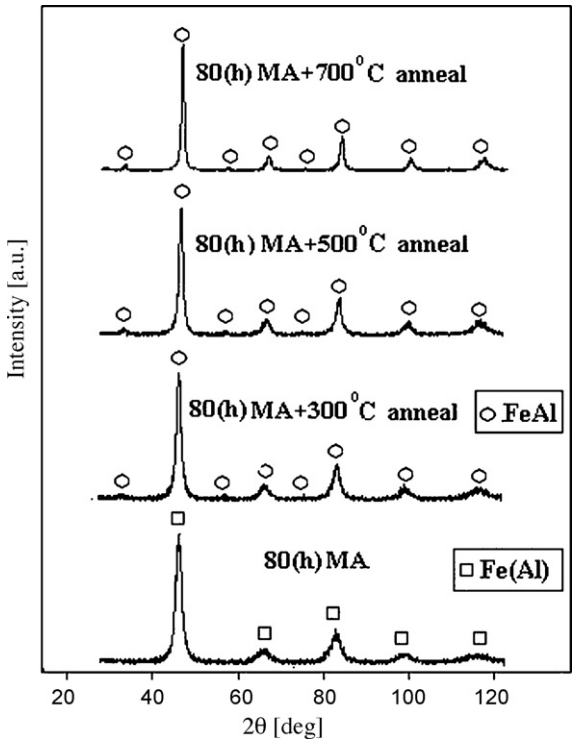

Fig. 8. XRD pattern of the powders milled for 80 h and annealed at 300, 500 and 700 °C.

graphs reflect that after 1 h MA, the layered structure consisting of Fe and Al is created; in contrast, in the powder milled for 15 min this structure is not observed. On the other hand, the observation of individual layers in the sample milled for 80 h is not possible and only the Fe(Al) solid solution persists according to the XRD analyses of Fig. 1.

The XRD patterns of the powder milled for 80 h and annealed for 1 h at 300, 500 and 700 °C are presented in Fig. 8. The comparison of the XRD patterns of the annealed powders with the as-milled powder reveals that the (1 0 0) and (1 1 1) superlattice reflections of the B2 structure appear, implying the ordering of the Fe(Al) solid solution and its transformation to the FeAl ordered intermetallic. In addition, all the peaks of the annealed powders are sharper than those of the as-milled powders. The lattice parameter, long-range order parameter, strain and crystallite size of these annealed samples are listed in Table 1, obtained from the analyses of the XRD data. It can be seen that during annealing, the crystallite size and long-range order parameter increase and the lattice parameter and strain decrease.

4. Discussion

4.1. MA of the Fe–50 at.% Al mixture

In the first stages of MA, the particles are plastically deformed and become flattened. By continuing the milling process, the par-

Table 1
Microstructural parameters of the annealed samples.

Long-range order parameter	Lattice parameter (Å)	Lattice strain (%)	Crystallite size (nm)	Annealing Temp. (°C)
0.49	2.903	2.215	19	300
0.77	2.898	1.685	26.68	500
0.82	2.896	1.2	38.5	700

ticles fracture due to work hardening. This leads to the creation of new surfaces which enabled the particles to weld together and form a layered structure consisting of the starting constituents. Due to the continued impact of the balls, the structure is steadily refined; consequently, the inter-layer spacing decreases and the number of layers in a particle increases. This gives rise to the enhanced diffusion of Al atoms into Fe lattice and the creation of zones in which Al atoms are dissolved in Fe lattice (Fe(Al)). After 20 h of MA, the primary Fe(Al) solid solution zones with the final composition are created (Fe(Al)). At this time, the Fe, Al and Fe(Al) phases exist together in the powders. With increasing the milling time to 50 h, retained Al atoms are dissolved in Fe lattice, leading to the growth of primary Fe(Al) solid solution zones and the increase of the crystallite size and lattice strain between 20 and 50 h of MA. Nevertheless, between 50 and 80 h milling, as shown in Fig. 5, the powder structure is refined and the lattice strain decreases because of severs plastic deformation, starting with the localization of deformation into shear bands with high dislocation density, which is followed by annihilation and recombination of dislocations forming subgrains that are transformed to grains [23]. After 80 h of MA, a steady state condition is obtained due to a balance between the dislocation accumulation and dynamic recovery through the formation of subgrain boundary and new grains. In addition, Fig. 3 shows that the lattice parameter of Fe(Al) is larger than that of Fe. This is due to the solution of Al atoms in Fe lattice; on the other hand, the increase in the Fe lattice parameter is related to an increase in Fe lattice defects during MA.

The deconvolution of the asymmetric diffraction peaks results in a more precise analysis of the phases. The powders milled for 5 and 10 h in which the intensity of Al(1 1 1) peak is considerable, Fe(2 1 1) peak is deconvoluted, because the ratio of the Fe-to-Al reflection intensity is the largest compared to other peaks [2]. For the samples milled for 20 and 30 h, all the peaks could be deconvoluted. Because the intensity of the strongest Al peak, (1 1 1), is very low; hence, the effect of other Al peaks on the intensity of the asymmetric peak could be neglected. In the powders milled for 50, 80 and 100 h, only one phase (Fe(Al)) exists; thus, no deconvolution of the peaks is needed.

4.2. Annealing

As tabulated in Table 1, annealing causes a decrease in the lattice strain and lattice parameter and an increase in the crystallite size and long-range order parameter. MA produces lattice defects, especially a high concentration of vacancies in this material. During annealing, movements of the excess vacancies in the lattice lead to the reordering of the structure and the decrease of the number of lattice defects, particularly in highly disordered regions. This reduces the lattice strain and enhances the long-range order parameter. Subsequently, by increasing the annealing temperature, the migration distances become larger and these excess vacancies get lost at grain boundaries or dislocation sinks which were produced during MA. This diffusion allows further ordering and a reduction in lattice parameter and strain [24]. Higher annealing temperature causes grain growth, since recovery and recrystallization processes occur faster and more time was available for grain growth [19].

5. Conclusion

1. MA of Fe and Al powders produced a micro-sandwich structure consisting of Fe and Al layers, then the structure was steadily refined and consequently the inter-layer spacing decreased. This led to an increase in the diffusion rate of Al atoms into Fe lattice and the creation of the Fe(Al) solid solution.
2. With increasing the milling time, the lattice parameter of the Fe(Al) phase increased due to the solution of Al atoms in Fe lattice and reached a steady value after 80 h milling.
3. The crystallite size and lattice strain of the Fe(Al) solid solution increased to 50 h of MA, then decreased between 50 and 80 h and remained nearly constant to 100 h.
4. Annealing of the powders led to the ordering of the Fe(Al) solid solution and its transformation to FeAl ordered phase. The higher the annealing temperature gave rise to the higher the order parameter.
5. During annealing, the crystallite size and long-range order of the FeAl phase increased and the lattice parameter and strain decreased.

References

[1] M. Krasnowski, T.J. Kulik, Intermetallics 15 (2007) 201–205.
[2] M. Krasnowski, A. Grabias, T. Kulik, J. Alloys Compd. 424 (2006) 119–127.
[3] R.N. Nogueira, C.G. Schon, Intermetallics 13 (2005) 1233–1244.
[4] S.C. Deevi, V.K. Sikka, C.T. Liu, Prog. Mater. Sci. 42 (1997) 177–192.
[5] Y.B. Pithawalla, M.S. El Shall, S.C. Deevi, Intermetallics 8 (2000) 1225–1231.
[6] J. Lapin, Mater. Sci. Eng. A 325 (2004) 163–176.
[7] N.S. Stoloff, V.K. Sikka, Physical Metallurgy and Processing of Intermetallic Compounds, Chapman and Hall, New York, 1996.
[8] D.D. Risanti, G. Sauthoff, Intermetallics 13 (2005) 1313–1321.
[9] C.C. Koch, Mechanical alloying, Mater. Sci. Forum 243 (1992) 88–90.
[10] H. Gleiter, Prog. Mater. Sci. 33 (1991) 223–315.
[11] I. Baker, Scripta Mater. 41 (1999) 409–414.
[12] D.G. Morris, M.A. Munoz-Morris, J. Chao, Intermetallics 12 (2004) 821–826.
[13] C Suryanarayana, Mechanical Alloying, Metals Handbook, vol. 7, 11th ed., ASM, Warrendale, 1998.
[14] C.C. Koch, Annu. Rev. Mater. Sci. 19 (1989) 121–143.
[15] K. Wolski, G. Le Caer, P. Delcroix, R. Fillit, F. Thevenot, J. Le Coze, Mater. Sci. Eng. A 207 (1996) 97–104.
[16] H.W. Shi, K. Guo, J. Alloys Compd. 455 (2008) 207–209.
[17] http://www.unipress.waw.pl/fityk [10 April 2007].
[18] G.K. Williamson, W.H. Hall, Acta Metall. (1953) 23–31.
[19] D.R. Askeland, The Science and Engineering of Materials, 3rd ed., PWS Publishing Co., Boston, 1994.
[20] JCPDS PDF card 33-0020.
[21] Q. Zeng, I. Baker, Intermetallics 14 (2006) 396–405.
[22] D.R. Amador, J.M. Torralba, J. Mater. Process. Technol. 143–144 (2003) 776–780.
[23] X. Amils, M.D. Baro, L. Lutterotti, J.S. Munoz, J. Nogues, S. Surinach, Nanostruct. Mater. 12 (1999) 801–806.
[24] X. Amils, J. Nogues, S. Surinach, M.D. Baro, Intermetallics 8 (2000) 805–813.